Pol. J. Environ. Stud. Vol. 28, No. 4 (2019), 2311-2319
DOI: *10.15244/pjoes/91076* ONLINE PUBLICATION DATE: 2019-01-18

Original Research

Synthesizing and Characterizing Sawdust Biochar/Fe_3O_4 Nanocomposites and its Potential Application in Textile Wastewater Treatment

Farah Nadeem, Nadia Jamil*, Amna Moazzam, Sajid Rashid Ahmad, Ambreen Lateef, Anam Khalid, Abdul Qadir, Azhar Ali, Soniya Munir

College of Earth and Environmental Sciences, University of the Punjab, Lahore, Pakistan

Received: 5 January 2018
Accepted: 15 May 2018

Abstract

The present research deals with the synthesis and viability of Sawdust biochar/Fe_3O_4 nanocomposite toward textile waste water treatment. The structure, functionality, and morphology of the nanocomposite were determined by FT-IR, powder XRD, and SEM. Removal of the textile dye Reactive Blue 21 (RB21) was almost 75% under optimum conditions. The value of Langmuir dimensionless separation factor R_L indicated a favorable adsorption ($0<R_L<1$). Langmuir constant (K_L, i.e., 0.15) symbolizes that there is high affinity of the adsorbent for the adsorbate. The value of Freundlich constant was found to be 2.78 ($n>1$), hence denoting favorable sorption. The negative values for free energy indicated a spontaneous reaction. Positive value for enthalpy suggested the endothermic nature of adsorption. The kinetic data showed a pseudo first-order kinetic model. The calculated value of q_t agreed with the experimental value of q_t at equilibrium. The results depicted that sawdust biochar/Fe_3O_4 nanocomposites are efficient adsorbents for removing RB21 and has potential application in treatment of textile wastewater.

Keywords: textile wastewater, nanocomposites, adsorption, biochar

Introduction

Azo and reactive dyes are mostly used in various industries like textile, leather, paper, food, plastic, and printing of color products [1-3]. Dyes are toxic for humans as well as the environment, and must be treated before their discharge to reduce environmental pollution [4]. Several methods for removing dyes include membrane filtration [5], coagulation/flocculation [6], advanced oxidation [7], and phyto-catalytic degradation [8]. Biodegradation of dyes is difficult because of their stable and complex chemical structure. Therefore, the adsorption process has been adopted for removal of dyes due to its simplicity, flexibility, ease of operation, and cost effectiveness [9].

Various adsorbents have been utilized for dye removal, such as alumina, rice husk, banana peels, orange peels, coconut shells, peanut shells, and various clays, etc. [10]. Among these, carbon-based materials are more efficient adsorbents, comprising large numbers of pores and high surface area for adsorption of dyes, but due to their high preparation cost they can't be used

*e-mail: ndnaveed@gmail.com

on a large scale [11, 12]. Plenty of research has been done on materials that can be used as raw materials for preparing low-cost charcoal [13], such as rice husk [14], seed shell [15], sawdust [16], coconut shell [17], pine cone [18], and wheat husk [19].

These either have low adsorption capacity when applied for actual wastewater or are ineffective for removing dyes. To enhance their effectiveness, charcoal is incorporated with different nano-materials for synthesizing nanocomposites [20]. Magnetic nanoparticles have seemed to show promising results with dyes. They can degrade and adsorb dyes from wastewater over a wide range of temperatures and pH values [11]. Charcoal with magnetic nanoparticles has been found to be more effective than other nanocomposites [21]. Simply put, it can be separated by external magnetic field from solution for reuse [22].

The current study is an attempt to synthesize Fe_2O_3/sawdust charcoal nanocomposite adsorbent for removing dyes from simulated textile effluent to reduce the environmental impacts of water pollution. Reactive blue 21 is a commonly used dye in textile industries and renders a strong color to the textile effluent. The use of such nanocomposites can be employed in industries as it will be a significant way forward for reducing water pollution and water waste caused by the textile industry.

Materials and Methods

Synthesizing Sawdust Biochar (SDB)

The sawdust was subjected to carbonization under anoxic conditions using a charcolator operated at atmospheric pressure. The sample at ambient temperature was placed in an aluminum container and heated at 300ºC for three hours. A 1 mm hole was drilled in the lid of the aluminum container so that steam and gas could escape to avoid any explosion during heating. After the carbonization was over, the container was left to cool for 30 minutes [23]. The prepared charcoal was soaked in distilled water for 2 hours and then boiled for one hour. It was then filtered, dried, ground to fine powder, and passed through a 60 mesh/inch sieve. The sieved sawdust biochar was stored in Ziploc polyethylene bags at room temperature until further experimentation.

Synthesizing Fe_3O_4/SDB Nanocomposite

The Fe_3O_4/SDB nanocomposite was synthesized by an in situ chemical co-precipitation method [24] in which SDB was used as support material. 20 g of SDB was added to 400 ml distilled water in a 1000 ml conical flask and stirred for 1 hr on a magnetic stirrer (MSH-20A WiseStir). In a separate beaker, 5.5602g of ferric sulphate ($FeSO_4.7H_20$) and 10.812g ferric chloride ($FeCl_3.6H_2O$) were dissolved in 200 ml distilled water and added in SDB suspension.100 ml of 0.8 M NaOH was taken in a separating funnel and added dropwise into the suspension of iron salts and SDB with continuous stirring. After dropping NaOH solution, the suspension was filtered and washed with a mixture of ethanol and water to clear all impurities and by products. The residue was dried in an oven (Memmert D-91126 SchwabachFRG) at 150ºC for 2 hours.

Characterization Techniques

The residual dye concentrations in aqueous solutions were determined by a UV-Vis spectrophotometer (752N, HEB, China). The prepared nanocomposite was characterized by Fourier transform infrared spectroscopy (FT-IR) to obtain information about the functional groups using a Fourier transform infrared spectrometer (Perkin Elmer spectrum RXI), scanning the sample in the wavelength range of 4000-700 cm^{-1}. A powder x-ray diffraction (XRD) study was conducted using a PANalyticalX'Pert Pro difffractometer. Diffraction data was attained by exposing samples to Cu-K_α x-ray radiation of wavelength (λ) 1.5418 Å. The sample was scanned for 20-80º2θ with step size of 0.05º2θ at 0.5 seconds per step size. Phase identification was carried out by means of MATCH! software in conjunction with the Crystallography Open Database. The surface morphology of the sample can was determined by scanning electron microscopy (Jeol JSM6480LV).

Batch Adsorption Studies: Kinetics, Thermodynamics, and Isotherms

The experiments of adsorption were carried out in 500 ml conical flask containing 30 ml of RB21 dye solution and 0.25 g of Fe_3O_4/SDB nanocomposite, with constant stirring at shaking speed of 200 rmp at different temperatures(10ºC, 30ºC, 50ºC, and 70ºC) in different time intervals (15, 30, 45, 60, 75, 90, and 105 minutes). Then the content of the experiment was filtered by Whatmann filter paper No. 41 to measure the Reactive Blue 21 (RB21) dye concentration in each sample using UV-Visible Spectrophotometer (752N, HEB, China) at λ_{max} = 621 nm by plotting the calibration curve. To study the effects of optimum parameter, experiments were carried out for different nanocomposite doses of 0.1, 0.15, 0.2, 0.25, 0.3, and 0.35 g/L at initial pH of 3, 5, 7, 9, and 11, and RB21 concentrations of 30, 60, 90, 120, 150, and 180 mg/L. Dye uptake efficiency was calculated using Eq. 1:

$$q\ (\text{mg/g}) = (C_i\text{-}C_e) \times V/M \quad (1)$$

…where q is the dye uptake by adsorbent (mg/g), and C_i and C_e are initial and final concentrations of RB21 dye, respectively. V is dye solution volume (1000 ml) and M is the mass of adsorbent used (grams).

The residual dye concentration in synthetic wastewater was calculated using Eq. 2:

$$R(\%) = (C_i\text{-}C_e) / C_i \text{ x } 100 \quad (2)$$

…where R is the residual dye concentration as a percentage, and C_i and C_e are initial and final concentrations of BR21 dye, respectively.

Isotherm models, including Langmuir and Freundlich models, were used to calculate equilibrium adsorption and to study surface properties and attraction of adsorbent toward the dye molecules [25]. The thermodynamic parameters were determined, and in order to explain the mechanism of adsorption of the solute on the adsorbent, the adsorption constants were calculated by pseudo first- and second-order mechanisms [26].

Results and Discussion

Characterization of Fe_3O_4/SDB Nanocomposite

The FT-IR spectra of synthesized nanocomposite shown in Fig. 1a) represents the peak at 799 cm^{-1}, which contributes to the Fe-O bond while other peaks appearing at 1119 cm^{-1} and 1380 cm^{-1} were due to the C-H bending and C-O stretching of the phenolic and methyl groups, respectively. Carbonyl vibrational stretching can be observed at 1901cm^{-1}. The peaks at 2005 cm^{-1} and 2325 cm^{-1} correspond to C=O bond and O=C=O stretching, respectively. The peak at 3218 cm^{-1} is attributed to O-H stretching, which could also be due to the moisture content in the adsorbent [27].

The powder XRD pattern of nanocomposite (Fig. 2a), indicates two distinct peaks depicting the presence of carbon between 2θ values of 22° and 26°, and of magnetite peak 36° as matched by the pattern [96-900-6922]. The nanocomposite was amorphous in nature, which depicts no or very little crystallinity. The SEM image of Fe_3O_4/SDB nanocomposite in Fig. 2b) (A and B) shows white color particles on SDB surface, which confirms the presence of Fe_3O_4.

Adsorption Capacity of Fe_3O_4/SDB Nanocomposite Toward Adsorption Capacity of Reactive Blue 21

The present study investigated the adsorption of RB21 on Fe_3O_4/SDB nanocomposite as a function of shaking speed, shaking time, adsorbent dose, pH,

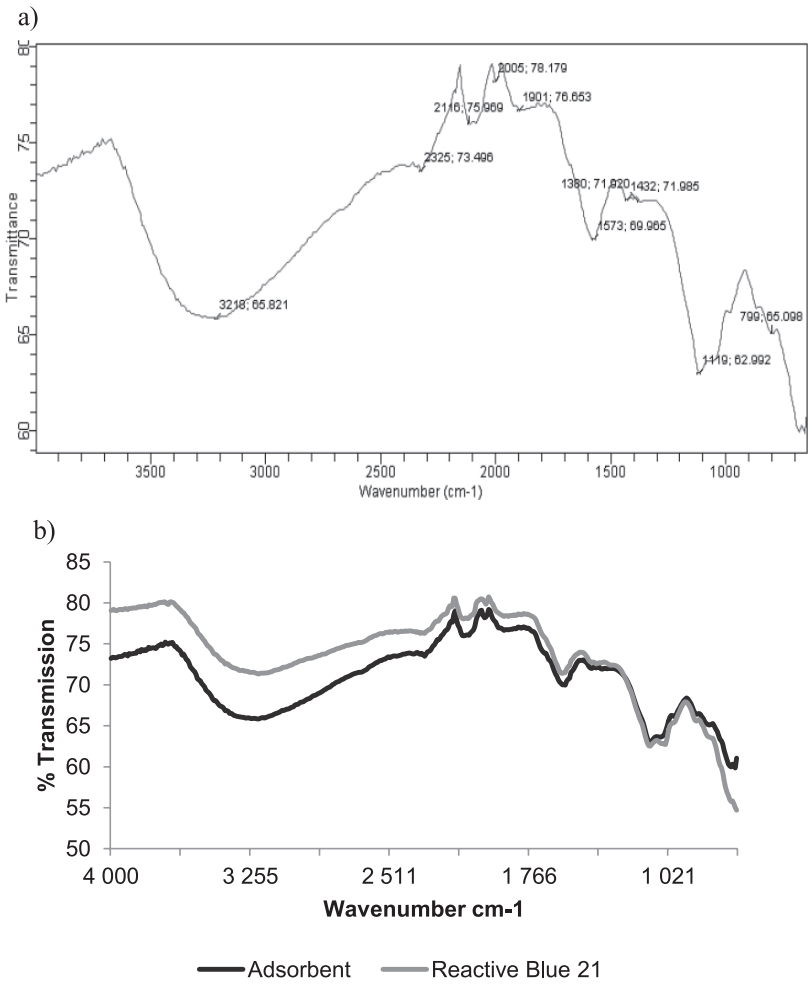

Fig. 1 a) FTIR spectra of Fe_3O_4/SDB nanocomposite; b) Comparison of FTIR spectra of Fe_3O_4/SDB nanocomposite before and after adsorption of RB 21dye.

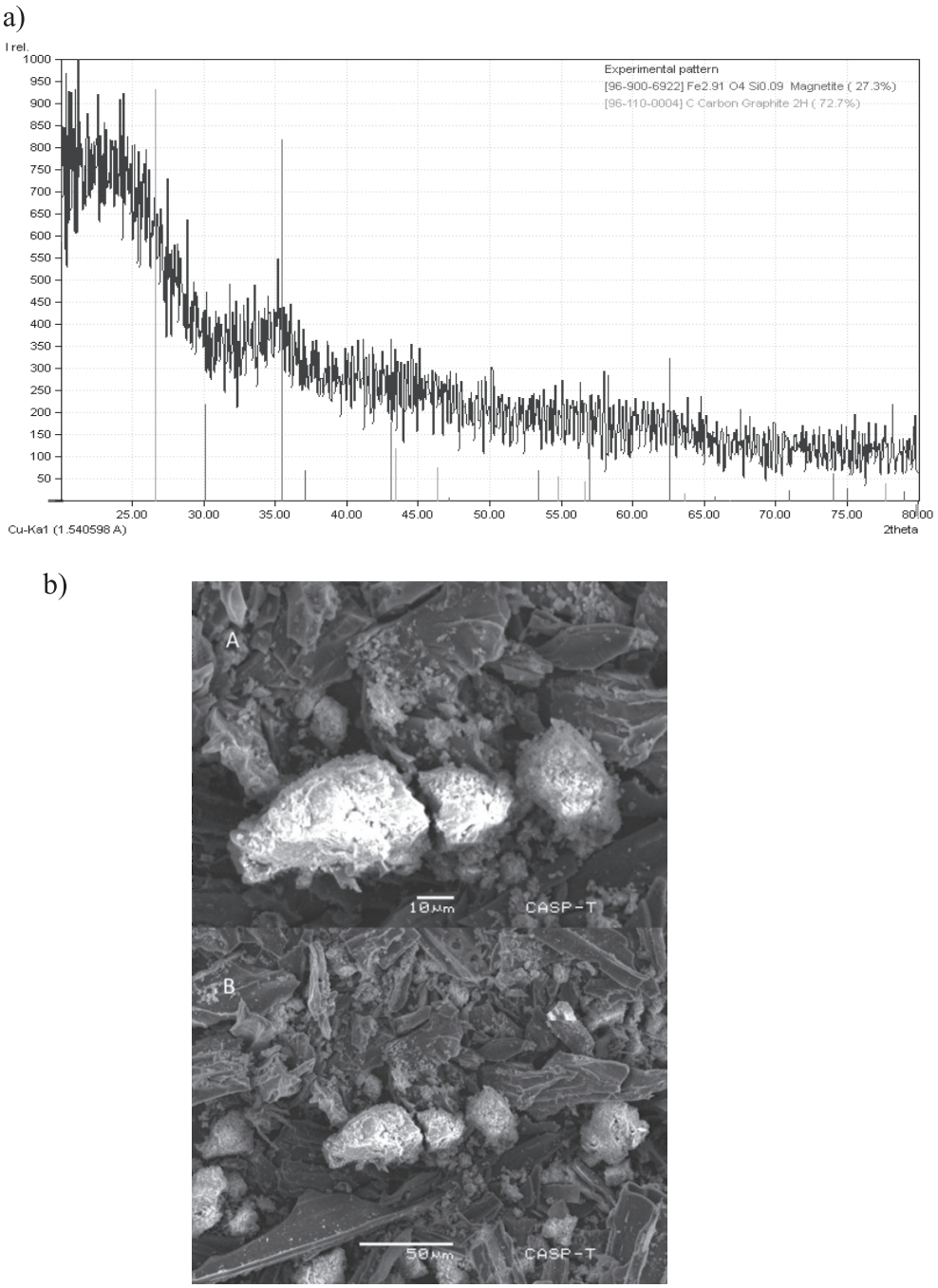

Fig. 2 a) Powder XRD pattern of Fe_3O_4/SDB nanocomposite along with COD reference pattern; b) SEM images of Fe_3O_4/SDB nanocomposite at 10µm (A) and 50µm (B) resolution showing white color particles on charcoal surface.

temperature, and effect of initial dye concentration. There was an increase in removal efficiency of RB21 with the increase in shaking speed, as shown in Fig. 3a). However, removal efficiency decreased when the shaking speed was increased past 200 rpm. The increase in adsorption with increase in agitation speed could be due to an increase in the mobility of the adsorption system. Resistance among the particles decreases and the adsorbate is moved toward the adsorbent. When the shaking speed is less, the adsorbent gets collected and does not spread, so a less active site will be available for the adsorbate to adhere. When there is sufficient speed, the sites on the surface of the adsorbent will be available to the dye [28]. However, after a certain speed (200 rpm in this case) there is a reduction in the adsorption, and desorption begins. This could be because there is more than the required increase in the kinetic energy of the molecules of the adsorbent as well as the dye, and they start hitting each other with greater force, which results in detachment of some dye molecules from the surface of the adsorbent [29].

The results in Fig. 3b) show an increase in removal efficiency of RB21 with the increase in shaking time,

but after 90 minutes there was no further improvement in adsorption capacity. This behavior of the adsorbent and dye could mean that high adsorption in the beginning could be due to the large number of sorption sites present at the earlier stage. A high concentration gradient between dye in solution and dye present on the surface of the adsorbent is developed. As the contact time increases, the number of active sites also decreases because they have been occupied by the adsorbate. When an optimum time is reached and maximum sites have been utilized, no further change in removal efficiency is observed [30].

We observed that removal efficiency of RB21 increased continuously with the increase in adsorbent dose as in Fig. 3c). This could be justified by the fact that the more the adsorbent, the more the number of sites present for adsorption. The adsorption sites do not saturate the adsorption system, hence increasing the dye uptake with an increase in adsorbent dose [31].

The effect of pH on adsorption of RB21 is shown in Fig. 3d), where the results depict maximum adsorption at neutral pH. The adsorption decreased in acidic and basic conditions. Similar results were obtained by some researchers [32] when using activated carbon to remove azo dyes. Highly acidic conditions led to an increase in amount of H+ ions, and the surface of the charcoal composite obtains a positive charge by absorbing those ions. The dye ions and the hydrogen ions hence get into a competition for the surface of the adsorbent, resulting in low adsorption of dyes due only to iron oxide

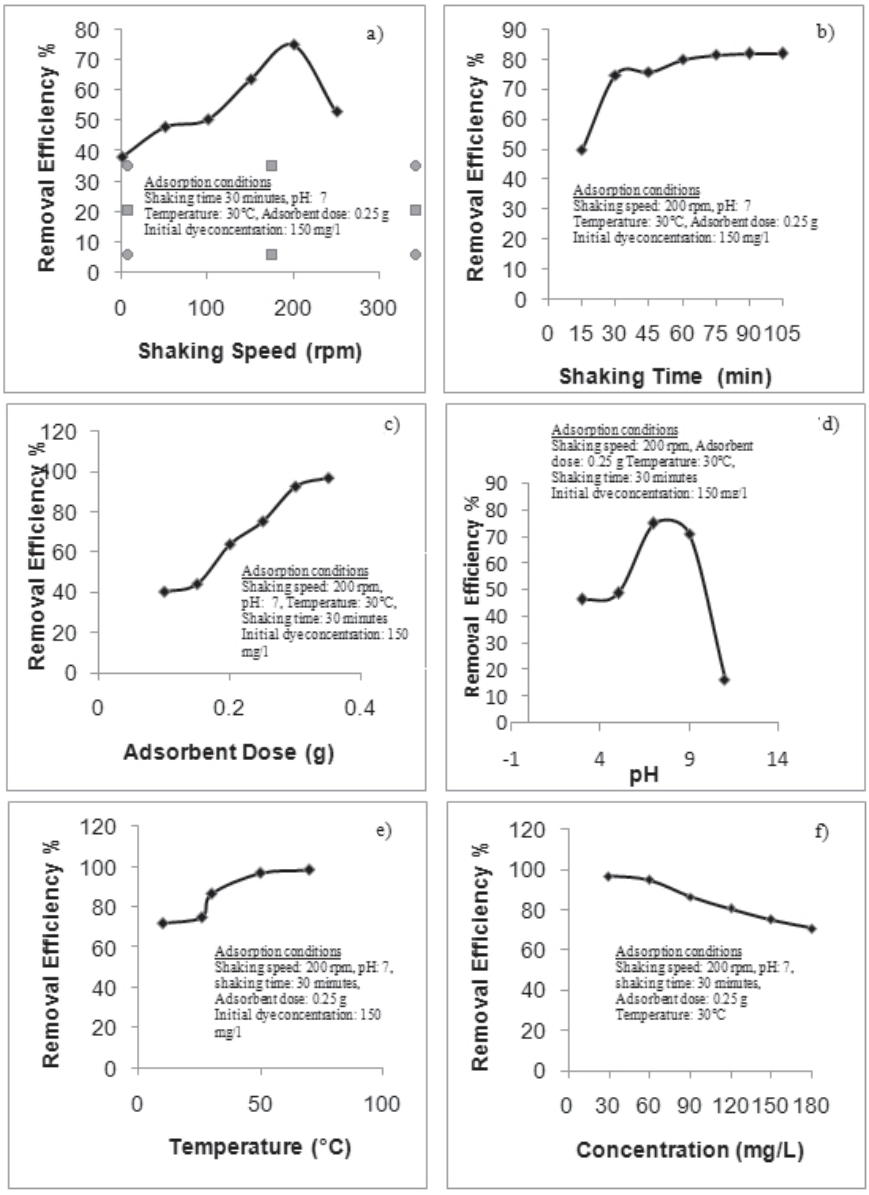

Fig. 3. Effects of: a) shaking speed on adsorption of RB21 on Fe_3O_4/SDB nanocomposite, b) shaking time on adsorption of RB21 on Fe_3O_4/SDB nanocomposite, c) adsorbent dose on adsorption of RB21 on Fe_3O_4/SDB nanocomposite, d) different pH on adsorption of RB21 on Fe_3O_4/SDB nanocomposite, e) varying temperature on adsorption of RB21 on Fe_3O_4/SDB nanocomposite, and f) initial dye concentration on adsorption of RB21 on Fe_3O_4/SDB nanocomposite.

nanoparticles. An increase in pH results in an increase in the negatively charged sites, and hence adsorption takes place only at the charcoal surface. So at neutral pH maximum adsorption took place [33].

The RB21 dye showed an increase in adsorption with the increase in temperature of the dye solution in Fig. 3e). The increase in adsorption along with temperature could be due to enhanced penetration of the dye. This also symbolizes that the adsorption of the dye was endothermic. A study by a group of researchers [34] also describes how such an increase in adsorption could be because of the creation of more active sites due to heat energy. A decrease in removal efficiency was noted with the increase in initial RB21 dye concentration, as shown in Fig. 3f). The adsorbent has a specific number of active sites for adsorption. Once the adsorbent becomes saturated, no further adsorption takes place. In the case of low dye concentrations, the numbers of binding sites increase, but with increasing dye concentration those sites fall short and hence adsorption capacity decreases [35].

Adsorption Isotherm Models

The Langmuir model [36] was calculated by Eq. 3:

$$C_e/q_e = 1/q_{max} \cdot C_e + 1/K_L \cdot q_{max} \quad (3)$$

…where q_{max} is the maximum amount of dye adsorbed per unit mass of adsorbent, and K_L is the Langmuir Constant. A linear plot of C_e/q_e against C_e was plotted and the values of q_{max} and K_L were obtained using the slope and intercepts of the plot.

The graph of specific sorption (Ce/qe) was plotted against equilibrium concentration for RB 21 in Fig. 4a). The linear plot for batch data with high coefficient of correlation (R^2) value for the dye revealed that the adsorption process obeyed the Langmuir isotherm model. The values of Langmuir constants, i.e., K_L, R_L, q_{max}, and R^2 are given in Table 1 for RB 21. Fig. 4b) shows variation of separation factor R_L with initial dye concentrations for RB 21. We observed from the graph that the separation factor decreases and nears zero with the increase in dye concentration. The value of Langmuir dimensionless separation factor R_L indicated favorable adsorption ($0< R_L<1$) [37] with a value of 0.04. We used the following equation for the Freundlich model [38]:

$$\log q_e = 1 / n \log C_e + \log K_f \quad (4)$$

…where K_f is the Freundlich constant. A linear plot of log q_e against log C_e was plotted and the values of n and K_f were obtained using the slope and intercepts of the plot.

The linear plot of log of amount adsorbed per amount of adsorbent at the equilibrium (log q_e) is plotted against the logarithm of equilibrium concentration (log C_e) for RB 21 in Fig. 4c). The linear plot for batch data with high coefficient of correlation (R^2) value revealed that the adsorption process obeyed the Freundlich isotherm model. The Freundlich constants were determined from the slope and intercept of the linear plot. The values of Freundlich constants, i.e., 1/n, n (adsorption intensity), K_f (adsorption capacity), and R^2 are given in Table 1.

Thermodynamic Models

The thermodynamic parameters were determined using the following Eqs. 5 and 6 [39] (ΔH° and ΔS° were determined from the slope and intercept of the linear Van't Hoff plot of lnK_{eq} versus 1/T):

$$\Delta G° = -RT\ln K \quad (5)$$

$$\text{and} \quad \ln K_{eq} = \Delta S°/R - \Delta H°/RT \quad (6)$$

… where ΔHº is enthalpy of adsorption, ΔSº is entropy change, ΔGº is Gibbs free energy change, R is the gas constant, T is absolute temperature, ln is the natural logarithm, and K_{eq} is the equilibrium constant.

Fig. 4d) shows the linear plots of lnK_{eq} against 1/T. The thermodynamic parameters for adsorption of RB 21 on Fe_3O_4/SDB nanocomposite are given in Table 2. The value of K_{eq} increased with temperature while Gibbs free energy (ΔG°) decreased with increasing temperature. The values obtained for ΔH° and ΔS° were positive for adsorption. The negative values for free energy indicated a spontaneous reaction. Positive value for enthalpy suggests the endothermic nature

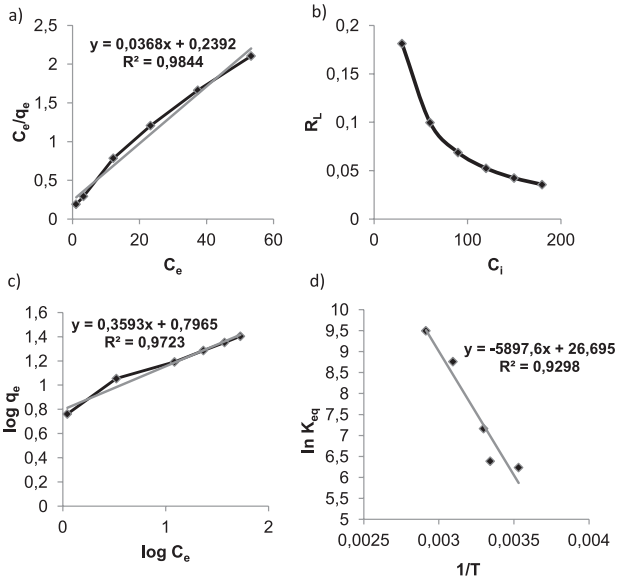

Fig. 4. a) Linear plot of Langmuir isotherm for adsorption of RB21 on Fe_3O_4/SDB nanocomposite, b) variation of separation factor (R_L) as a function of initial concentration of RB21, c) linear plot of Freundlich isotherm for adsorption of RB21 on Fe_3O_4/SDB nanocomposite, and d) graph of lnK_{eq} versus 1/T for adsorption of RB21.

Table 1. Adsorption isotherm parameters for RB21 onto Fe_3O_4/SDB nanocomposite (bold values are experimental finding results).

Model_	Parameters_ $q_{max,exp}$ (mg/g)	Value 25.334
Langmuir	$q_{max,cal}$ (mg/g)	27.77778
	K_L (L/mg)	0.150627
	R_L	0.042383
	R^2	0.775
Freundlich	N	2.785515
	K_f	6.251727
	R^2	0.972

Table 2. Thermodynamic parameters (ΔH°, ΔG°, ΔS°) for the adsorption of Reactive Blue 21.

Temperature (°C)	K_{eq}	ΔG° (Jmol$^-$)	ΔH° (Jmol$^-$)	ΔS° (Jmol$^-$K$^-$)
10	510.5637	-14679.1	49.027658	221.73
26	594.0709	-15885.3		
30	1291.795	-18055.5		
50	6378.947	-23537.3		
70	13313.51	-27093.1		

of the adsorption. Also, ΔH° was found to be greater than 40 KJ/mol, symbolizing the chemisorption of RB 21 on the adsorbent. Positive values for ΔS° indicated an increase in randomness during the adsorption process [40].

Kinetic Models

The following Eq.7 was used for the pseudo first-order mechanism:

$$\log (q\text{-}q_e) = \log q - k_1 t/2.303 \qquad (7)$$

…where q is the amount of dye adsorbed at equilibrium (mg/g), q_e is the amount of dye adsorbed at time t (mg/g), and K_1 is the equilibrium rate constant of pseudo first-order sorption (min^{-1}).

A linear plot of log ($q\text{-}q_e$) was plotted against time (t). The values of rate constant (K_1), coefficient of correlation (R^2), and $q_{calculated}$ were found using slope and intercept of the graph.

The following equation was used for the pseudo second order mechanism:

$$t/q = 1/k_2 q_e^2 + t/q \qquad (8)$$

… where q is the amount of dye adsorbed at equilibrium (mg/g), q_e is the amount of dye adsorbed at time t (mg/g),

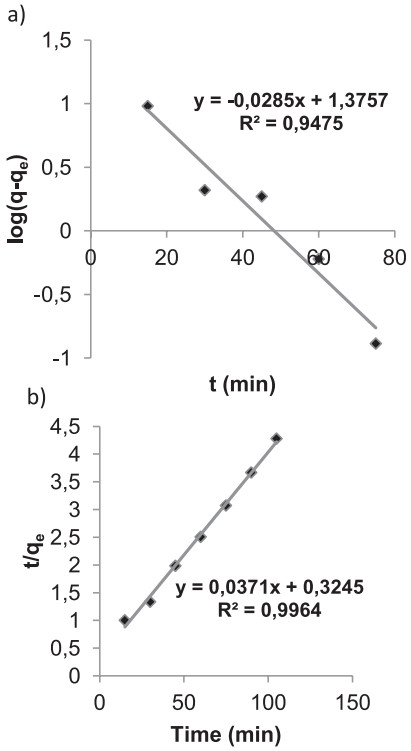

Fig. 5. a) Pseudo first-order sorption kinetics of RB21 on Fe_3O_4/SDB nanocomposite, and b) pseudo second-order sorption kinetics of RB21 on Fe_3O_4/SDB nanocomposite.

Table 3. Kinetic model parameters for the adsorption of RB21 onto Fe_3O_4/SDB nanocomposite (bold values are experimental finding results).

Model_	Parameters_ $q_{max,exp}$ (mg/g)	Value 24.534
Pseudo-first order	$q_{max,cal}$ (mg/g)	23.71374
	K_1 (min^{-1})	0.06445
	R^2	0.947
Pseudo-second order	$q_{max,cal}$ (mg/g	27.02703
	K^2	0.00423
	R^2	0.996

K_2 is the equilibrium rate constant of pseudo first-order sorption min^{-1}, and h = $k_2 q^2$ – where h is the initial sorption rate and mg g^{-1}min^{-1}. A linear plot of log t/q_e was plotted against time (t). The values of rate constant (K_2), coefficient of correlation (R^2), and $q_{calculated}$ were found using slope and intercept of the graph.

The adsorption rates were calculated using pseudo first-order and pseudo second-order kinetics models. The log(q/q_e) plotted against time is shown in Fig. 7a). The linear plot and high coefficient of correlation (0.947) confirms the application of first-order kinetics. Fig. 7b) shows the plot of t/q_e against time. The linear plot and high coefficient of correlation (0.996) confirms the application of second-order kinetics as

well. The value of calculated dye uptake at equilibrium for first-order kinetics is very close to the experimental value as opposed to the calculated value of second-order kinetics, hence the batch data for RB 21 best fit first-order kinetics. The kinetic parameters for adsorption on Fe_3O_4/SDB nanocomposite are given in Table 3.

Adsorption Mechanism

Fig. 1b) shows FT-IR spectra of nanocomposite after adsorption of dye, revealing that the intensity of the peaks has altered and that peak width has varied at some points. For RB21, the involvement of the major functional groups can be observed due to the change in intensity of the peaks. The transmission for almost all peaks has increased, indicating a decrease in intensity. Weak electrostatic forces or Vander Wall forces could be responsible for this adsorption, and some chemisorption has also occurred due to changes in the thickness of certain peaks

Conclusions

It may be concluded that the proposed method is a simple and cost-effective way to synthesize Fe_3O_4/SDB nanocomposite for the efficient removal of RB21 from textile effluent. 75% color removal was attained at 90 minutes shaking with adsorbent dose of 0.25 g and initial dye concentration of 150 mg/L. The shaking speed was set at 200 rpm for 30 minutes at 30ºC and neutral pH. The pseudo first-order and pseudo second-order kinetics, Langmuir and Freundlich isotherms, and thermodynamics revealed that the adsorption process was chemisorption. The negative values for free energy indicated a spontaneous reaction. Positive value for enthalpy suggests the endothermic nature of adsorption. The kinetic data obeyed a pseudo first-order kinetic model. The calculated values of q_t agreed with the experimental value of q_t at equilibrium. Hence, the results represent that Fe_3O_4/SDB nanocomposites can be used for the efficient removal of RB21 from wastewater. This research is a significant way forward toward the treatment of textile wastewater and can be used as a baseline for further innovation and development.

Conflict of Interest

The authors declare no conflict of interest.

References

1. ASGHER M. Biosorption of reactive dyes: a review. Water Air Soil Pollut. **223** (5), 2417, **2012**.
2. FAGUNDES-KLEN M.R., CERVELIN P.C., VEIT M.T., GONCALVES G.C., BERGAMASCO R., DA SILVA F.V. Adsorption kinetics of blue 5G dye from aqueous solution on dead floating aquatic macrophyte: effect of pH, temperature, and pretreatment. Water Air Soil Pollut. **223** (7), 4369, **2012**.
3. SHIRZAD S.M., SAMARGHANDI M., AZIZIAN S., KIM W., LEE S. The removal of hexavalent chromium from aqueous solutions using modified holly sawdust: equilibrium and kinetics studies. Environmental Engineering Research. **16** (2), 55, **2011**.
4. MAKARCHUK O.V., DONTSOVA T.A., ASTRELIN I.M. Magnetic nanocomposites as efficient sorption materials for removing dyes from aqueous solutions. Nanoscale Res Lett. **11** (1), 161, **2016**.
5. YU S., CHEN Z., CHENG Q., LU Z., LIU M., GAO C. Application of thin-film composite hollow fiber membrane to submerged nanofiltration of anionic dye aqueous solutions. Sep Purif Technol. **88**, 121, **2015**.
6. VERMA A.K., DASH R.R., BHUNIA P. A review on chemical coagulation/flocculation technologies for removal of colour from textile wastewater. Journal of Environmental Management. **93** (1), 154, **2012**.
7. CUIPING B., XIANFENG X., WENQI G., DEXIN F., MO X., ZHONGXUE G., NIAN X. Removal of Rhodamine B, by ozone-based advanced oxidation process. Desalination. **278** (1), 84, **2011**.
8. PATIL B.N., NAIK D.B., SHRIVASTAVA V.S. Photocatalytic degradation of hazardous Ponceau-S dye from industrial wastewater using nanosized niobium pentoxide with carbon. Desalination. **269** (1), 276, **2011**.
9. FARROKHI M., HOSSEINI S.C., YANG J.K., SHIRZAD-SIBONI M. Application of ZnO–Fe_3O_4 Nanocomposite on the removal of azo dye from aqueous solutions: kinetics and equilibrium studies. Water Air Soil Pollut. **225** (9), 2113, **2014**.
10. JAIN R., SHARMA N., RADHAPYARI K. Electrochemical treatment of pharmaceutical azo dye amaranth from wastewater. J. Appl. Electrochem. **39** (5), 577, **2009**.
11. TAN I.A.W., AHMAD A.L., HAMEED B.H. Adsorption of basic dye using activated carbon prepared from oil palm shell: batch and fixed bed studies. Desalination. **225** (1-3), 13, **2008**.
12. DE YUSO A.M., RUBIO B., IZQUIERDO M.T. Influence of activation atmosphere used in the chemical activation of almond shell on the characteristics and adsorption performance of activation carbon. Fuel Processing Technology. **119**, 74, **2014**.
13. GUPTA V.K. Application of low-cost adsorbents for dye removal – A review, Journal of Environmental Management. **90** (8), 2313, **2009**.
14. GUPTA V.K., MITTAL A., JAIN R., MATHUR M., SIKARWAR S., Adsorption of Safranin-T from wastewater using waste materials - activated carbon and activated rice husks. J. Colloid Interface Sci. **303** (1), 80, **2006**.
15. THINAKARAN N., PANNEERSELVAM P., BASKARALINGAM P., ELANGO D., SIVANESAN S. Equilibrium and kinetic studies on the removal of acid red 114 from aqueous solutions using activated carbons prepared from seed shells, J Hazard Mater. **158** (1), 142, **2008**.
16. VIJAYARAGHAVAN K., WON S. W., YUN Y. Treatment of Complex Remazol Dye Effluent Using Sawdust- and Coal-Based Activated Carbons. J Hazard Mater. **167** (1), 790, **2009**.
17. SHARMA Y.C., UPADHYAY S.N.U. Removal of a cationic dye from wastewaters by adsorption on activated

carbon developed from coconut coir. Energy Fuels. **23** (6), 2983, **2009**.
18. MAHMOODI N.M., HAYATI B., LAN C. Adsorption of textile dyes on pine cone from colored wastewater: kinetic, equilibrium and thermodynamic studies. Desalination. **268** (1), 117, **2011**.
19. SAHA P.D., DEY A., MARIK P. Batch removal of chromium (VI) from aqueous solutions using wheat shell as adsorbent: process optimization using response surface methodology. Desalin Water Treat. **39** (1-3), 95, **2012**.
20. TAN X.F., LIU Y.G., GU Y.I., XU Y., ZENG G.M., HU X.J., LIU S.B., WANG X., LIU S.M., LI J. Biochar-based nanocomposites for the decontamination of wastewater: A review. Bioresour Technol. **212**, 318, **2016**.
21. XU P., ZENG G.M., HUANG D.L., FENG C.L., HU S., ZHAO M.H., LAI C., WEI Z., HUANG C., XIE G.X., LIU, Z. F. Use of iron oxide nanomaterials in wastewater treatment: a review. Sci Total Environ. **424**, 1, **2012**.
22. ZHANG M., GAO B. Removal of arsenic, methylene blue, and phosphate by biochar/AlOOH nanocomposite. Chemical Engineering Journal. **226**, 286, **2013**.
23. BRAADBAART F., POOLE I., HUISMAN H.D., VAN OS B. Fuel, fire and heat: an experimental approach to highlight the potential of studying ash and char remains from archaeological contexts. J. Archaeol. Sci. **39** (4), 836, **2012**.
24. PEREZ G. Morphology Control of Iron Oxide Nanoparticles Produced by Co-precipitation. Microscopy and Microanalysis. **18** (S2), 250, **2012**.
25. SHARMA P., DAS M.R. Removal of a cationic dye from aqueous solution using graphene oxide nanosheets: investigation of adsorption parameters. J. Chem. Eng. Data. **58** (1), 151, **2012**.
26. AI L., LI M., LI L. Adsorption of methylene blue from aqueous solution with activated carbon/cobalt ferrite/ alginate composite beads: kinetics, isotherms, and thermodynamics. J. Chem. Eng. Data, **56** (8), 3475, **2011**.
27. BOJIC D.V., RANDELOVIC M.S., ZARUBICA A.R., MITROVIC J.Z. RADOVIC M.D., PURENOVIC M.M., BOJIC A.L., Comparison of new biosorbents based on chemically modified Lagenaria vulgaris shell. Desalin Water Treat, **51** (34-36), 6871, **2013**.
28. MADRAKIAN T., AFKHAMI A., MAHMOOD-KASHNI H., AHMADI M. Adsorption of some cationic and anionic dyes on magnetite nanoparticles-modified activated carbon from aqueous solutions: equilibrium and kinetics study. J. Iran. Chem. Soc. **10** (3) 481, **2013**.
29. LO S.F., WANG S.Y., TSAI M.J., LIN L.D. Adsorption capacity and removal efficiency of heavy metal ions by Moso and Ma bamboo activated carbons. Chem. Eng. Res. Des. **90** (9), 1397, **2012**.
30. STANKOVIC V., BOZIC D., GORGIEVSKI M., BOGDANOVIC G. Heavy metal ions adsorption from mine waters by sawdust. Chemical Chem. Ind. Chem. Eng. Q. **15** (4), 237, **2009**.
31. WANG H., SHEN Y., SHEN C., WEN Y., LI H. Enhanced adsorption of dye on magnetic Fe_3O_4via HCl-assisted sonication pretreatment. Desalination. **284**, 122, **2012**.
32. RAO A.N., LATHASREE S., SIVASANKAR B., SADASIVAM V., RENGARAJ K. Removal of azo dyes from aqueous solutions using activated carbon as an adsorbent. J Environ Sci Eng. **46** (2), 172, **2004**.
33. WANG X., ZHU N., YIN B. Preparation of sludge-based activated carbon and its application in dye wastewater treatment. J Hazard Mater. **153** (1), 22, **2008**.
34. AL-DEGS Y.S., EL-BARGHOUTHI M.I., EL-SHEIKH A.H., WALKER G.M., Effect of solution pH, ionic strength, and temperature on adsorption behavior of reactive dyes on activated carbon. Dyes Pigments. **77** (1), 16, **2008**.
35. BHATNAGAR A., MINOCHA A. Conventional and non-conventional adsorbents for removal of pollutants from Water. Indian J. Technol. **13**, 203, **2006**.
36. BOSTROM M., LIMA E.R.A., TAVARES F.W., NINHAM B.W. The influence of ion binding and ion specific potentials on the double layer pressure between charged bilayers at low salt concentrations. J. Chem. Phys. **128** (13), 04B604, **2008**.
37. ZHENG H., LIU D., ZHENG Y., LIANG S., LIU Z. Sorption isotherm and kinetic modeling of aniline on Cr-bentonite. J Hazard Mater. **167** (1), 141, **2009**.
38. TANHAEI B., AYATI A., LAHTINEN M., SILLANPAA M. Preparation and characterization of a novel chitosan/ Al_2O_3/ magnetite nanoparticles composite adsorbent for kinetic, thermodynamic and isotherm studies of Methyl Orange adsorption. Chem. Eng. J. **259**, 1, **2015**.
39. KONSTANTINOU I.K., ALBANIS T.A. Adsorption-desorption studies of selected herbicides in soil-Fly ash mixtures. J. Agric. Food. Chem. **48** (10), 4780, **2000**.
40. IQBAL M.J., ASHIQ M.N. Thermodynamics of adsorption of dyes from aqueous media on activated charcoal. Journal of Research in Science. **18** (2), 91, **2007**.